PAPER

Check for updates

Gold nanoparticles functionalized by phosphine oxide derivatives: characterization and influence of ligand structure on their stability†

Wanisa Abdussalam-Mohammed, [iD] *[a] Mashael M. Alshaikh, [iD] [b] Pawan Shah [iD] [c] and Ajaya Bhattarai [iD] *[d]

The rapid development of nanotechnology has led to an incredible expansion in the production and use of nanoparticles (NPs). Gold nanoparticles (AuNPs) are one of the most significant types of NPs and have shown outstanding medical applications due to their low toxicity. AuNPs stabilized by phosphine derivatives have extensive applications in sensing, catalysis, and biological imaging. In this work, phosphine oxide ligands were employed to stabilize AuNPs in DMSO with $NaBH_4$ as the reducing agent. These ligands included (3-thioacetyl-*N*-ethylmethylamine)-diphenylphosphine oxide (**10**), (3-thioacetylpropyl)-thiodiphenylphosphine oxide (**7**), (3-thioacetylpropyl)di-(*p*-tolyl)phosphine oxide (**4A**), and (3-thioacetylpropyl)-diphenylphosphine oxide (**4B**). The AuNPs were characterized by transmission electron microscopy (TEM), dynamic light scattering (DLS), and UV-Vis spectroscopy. AuNPs stabilized by both **4B** and **7** remained stable for five months. However, when **4A** and **10** were used, the AuNPs remained stable for three months. Due to their small surface-area-to-volume ratio and good stability, AuNPs are nowadays needed for different applications. Therefore, small, homogenous, and spherical AuNPs were considered herein, where their sizes were 55 ± 13.6 nm, 40 ± 8 nm, 25 ± 6 nm, and 43 ± 7 nm for **4A**-AuNPs, **4B**-AuNPs, **7**-AuNPs, and **10**-AuNPs, respectively, based on TEM results. These results aligned with the DLS results, where homogenous AuNPs were produced with no evidence of aggregation.

1. Introduction

Light is absorbed by noble metal nanoparticles, such as gold, silver, or copper, due to the excitation of localized surface plasmon resonance (LSPR).[1] For example, gold nanoparticles (AuNPs) gained attention as a potential material for producing hot carriers in photocatalysis and have been utilized in electrochemical capacitors.[2] In addition, numerous medical applications use AuNP formulations as contrast agents for computed tomography (CT) scans and as agents for photothermal ablation of tumors.[3] Recently, AuNPs have shown many applications across several medical domains, such as cancer, ocular diseases, cardiovascular diseases, and diabetes.[4] For many applications, particularly bio-applications, the surface

modification and protection of AuNPs are crucial prerequisites.[5] It is beneficial to add functionality to gold nanoparticles for specific purposes. Recently, AuNPs have gained popularity due to their potential application in photothermal therapy. Heat is generated on the surface of an AuNP when light is absorbed, primarily due to electron–electron scattering and the coupling of electrons with lattice vibrations.[6] Creating biological ligands to effectively identify and bind tumor cells to metals is one problem related to the core–shell structure of particles. Thus, it is necessary to have metal nanoparticles (NPs) that can distinguish between various kinds of cancer cells. It has been shown that cells accumulated phosphonium-functionalized gold nanoparticles (AuNPs) and TEM verified their presence in the mitochondria.[7]

It is known that AuNPs can be synthesized using different techniques based on their size and shape requirements. Among those methods are laser ablation, Brust, Turkevich, and seed-mediated growth methods. For example, AuNPs with a size 7.6 nm were prepared by laser ablation in a liquid, where a small amount of aggregation occurred due to the absence of capping agents in this method.[8]

Furthermore, AuNPs prepared *via* the Turkevich approach are 1–2 nm in size. In this process, reducing gold ions (Au^{3+}) to Au^0 yields gold nanoparticles (NPs). AuNPs of certain sizes,

[a]Chemical Engineering Department, Faculty of Engineering, University of Tripoli, Tripoli, Libya. E-mail: w.ahweelat@uot.edu.ly

[b]Physical Department, Al Jumum University College, Umm Al-Qura University, Makkah, Saudi Arabia

[c]Central Department of Chemistry, Tribhuvan University, Kirtipur, Nepal

[d]Department of Chemistry, Mahendra Morang Adarsh Multiple Campus, Tribhuvan University, 15 Biratnagar, Nepal. E-mail: bkajaya@yahoo.com; ajaya.bhattarai@mmamc.tu.edu.np

† Electronic supplementary information (ESI) available. See DOI: https://doi.org/10.1039/d5na00111k

ranging from 16 to 147 nm, were prepared by adjusting the ratio of stabilizing and reducing agents. In addition, AuNPs with a size range of 1.5–5.2 nm were generated by the Brust method using two-phase organic solvents, where sodium borohydride was used as a reducing agent. Both Turkevich and Brust methods produce only spherically shaped AuNPs. In contrast, the most popular method for creating rod-shaped AuNPs is seed-mediated growth. This technique is based on the idea that seed particles are initially synthesized by reducing gold salts.[9]

The use of various capping/stabilizing agents to stabilize AuNPs is a key objective. For instance, stabilized ligands with Au–P bonding are comparatively weaker than those with Au–S bonding. As a result, thiolate-stabilized Au clusters and Au–phosphine clusters differ significantly in their chemistry, structure, and physical characteristics. Furthermore, strong Au–S bonds play a key role in stabilizing assemblies capped with thiolates on gold nanoparticle surfaces.[10] Compared to weakly bound systems like nitrogen–Au and phosphine–Au, the interaction between gold and sulfur is the most studied gold organic system found in the literature.[10,11] For instance, thiol/phosphine ligands applied as protective ligands have significantly improved AuNP management during the last few decades.[11] Ligands have different affinities toward the NP surface, which are dependent on the ligand head groups and the nature of the NP surface. Additional sulfur functional groups like S-thiocarbamates (RSC(=O)NR$_2$, thioesters) and thiocarbamates (O-thiocarbamates, (ROC(=S)NR$_2$) (esters)) have been applied as stabilizing agents for a range of metal nanoparticles (MNPs). However, they showed less affinity for the surface of the MNPs compared to thiol functional groups.[12,13] Organic groups, such as amine derivatives, are commonly used to stabilize metal nano particles. The primary distinction between thiol and amine functions is the stability of the NPs. Additionally, AuNPs, stabilized by amine group-containing ligands are bigger than those containing thiol group ligands. The weak interactions between amines and AuNPs were due to the amine groups' low affinity for the AuNP surface. However, amine and thiol groups can both work well together. For example, peptides and AgNPs are connected through both amine and thiol functionalities.[14,15]

According to the literature, AuNPs modified with cavitands demonstrated exceptional stability due to the incorporation of two thiol groups. In contrast, AuNPs prepared with two amine-based cavitands showed a tendency to agglomerate quickly.[16] Furthermore, AuNPs with various electrical characteristics have been functionalized in the presence of NaBH$_4$ and secondary phosphine oxides (SPOs), where tiny sized AuNPs (1.2–2.2 nm) were generated.[17] The hydrogenation of aldehyde derivatives was also more actively catalyzed by AuNPs, functionalized by aryl-substituted SP=Os than by those containing alkyl SP=Os, which demonstrated moderate activity. This difference occurred as a result of the strongly polar nature of the P=O bonds of aromatic SP=Os attached to AuNPs.[18] Phosphine oxide synthesis can be very beneficial because of the ability of phosphine oxide to form hydrogen bonds with biomolecules.

For instance, R–P(O)(OH)$_2$ and 11-mercaptoundecanylphosphonic acid, exhibit a wide spectrum of biological activities, including the ability to block enzymes. Similarly, through the oxygen in the P=O bond, phosphonic acid groups can function as electron acceptors, while their P–OH group will enable hydrogen bonding.[19] Furthermore, NaBH$_4$ and *tert*-butyl(naphthalen-1-yl)phosphine oxide have been used to functionalize an air-stable and homogenous AuNP.[20] Other stabilizers, such as 1,1,1-tris (diphenylphosphinomethyl)ethane CH$_3$C[CH$_2$P(C$_6$H$_5$)$_2$]$_3$ and 1,1,1-tris-(diphenylphosphinomethyl) ethane trisulfide [CH$_3$C(CH$_2$P(S)(C$_6$H$_5$)$_2$)$_3$], stabilize AuNPs, create small sizes, and provide important bio applications. Those AuNPs were efficient against Gram-positive bacteria than against Gram-negative bacteria.[21] Both sulfur and phosphorus are found to be the best donor atoms toward a variety of metals. Phosphino-thiols include phosphine moieties and thiol groups that are linked by an organic molecular bond; for instance, phosphinothioformamides have been utilized in catalytic processes.[22]

As previously indicated, the stability of AuNPs is crucial for their use in a variety of domains, including bioassays, catalysis, and nano-optoelectronics. Therefore, a variety of ligands, such as thiol, disulfide, phosphine oxide (P=O), amine, phosphine, and carboxylate, have been selected to stabilize AuNPs.[23]

Furthermore, gold nanorods stabilized with bidentate N-heterocyclic-carbene-thiolate ligands were stable at low temperature, high salt concentration, over a broad pH range, and under gold etching conditions. These gold nanorods worked well for photothermal treatment (PTT) *in vitro*.[24] Furthermore, amine and phosphine ligands were used to modify the physical and chemical properties of the AuNPs, such as solubility and light absorption.[25] Therefore, our ligands were chosen for their ability to stabilize AuNPs for potential future uses.

2. Experimental

Every chemical used in this study was acquired from Fisher Scientific Ltd. and Sigma-Aldrich. No additional purification was required; all reagents were used exactly as provided.

2.1 UV-visible spectroscopy

A PerkinElmer Lambda 19 UV/Vis/NIR spectrophotometer was used for analyzing the AuNP samples, and UV-Vis absorption spectra were noted at R.T. in the 200–800 nm range. The solvent used to dissolve the relevant sample was also used to correct all data for background absorption.

2.2 Transmission electron microscopy

A Tecnai-12 device running at 100 kV accelerating voltage was used to create Transmission electron microscopy (TEM) micrographs. The sample was centrifuged at 4000 rpm. One drop of the reaction mixture from the centrifuged solution was placed on a copper grid coated with 150 mesh Formvar. After that, the grid was left to dry before it was photographed. ImageJ and OriginPro 2018 were used to analyze at least 170 particles in the TEM images to investigate particle size.

2.3 Dynamic light scattering

The size of the gold nanoparticles was measured using a Malvern Zetasizer Nano ZS (UK) instrument, which had a scattering detector at 173° and a HeNe laser operating at 633 nm. The measurements were taken at 25 °C. The samples were transferred to a quartz cuvette, where the measurements were taken for each sample. Additionally, ImageJ software was used for graphical purposes.

2.4 Cationic phosphonium ligand synthesis

The production of (3-thioacetylpropyl) diphenylphosphine oxide (**4B**) was carried out according to a documented process.[26,27] In contrast, the synthesis and characterization of (3-thioacetylpropyl)di-(p-tolyl)-phosphine oxide (**4A**), (3-thioacetylpropyl)thiodiphenylphosphine oxide (**7**), and (3-thioacetylethyl-N-methylamine)diphenylphosphine oxide (**10**) were previously unreported.

2.4.1 Preparation of (3-thioacetylpropyl)di-(p-tolyl)phosphine oxide (4A) and (3-thioacetylpropyl)diphenylphosphine oxide (4B). Scheme 1 illustrates the production of phosphine oxide (**4A** and **4B**). The compounds were initially obtained through basic hydrolysis of hydroxypropylphosphonium salt (compound **2**), yielding (hydroxypropyl)-di(p-tolyl)phosphine

oxide in the case of the tolyl ring (**2A**) and (hydroxypropyl)-diphenylphosphine oxide in the case of the benzene ring (**2B**).

After dissolving the hydroxylpropylphosphonium salt (**1A/1B** 1 mmol) in ethanol (1.5 ml), the solutions were heated to 50 °C with 2 ml of 20% NaOH solution. The corresponding amount of bromopropylphosphine oxide (**3A/3B**) was obtained by dissolving **2A/2B** in HBr (48%, 5 ml) and refluxing the mixture for five hours. In the last step, potassium thioacetate (3 mmol) and bromopropylphosphine oxide (**3A/3B**, 2 mmol) were reacted in 5 ml of ethanol. To obtain **4A/4B**, the mixture was stirred under nitrogen overnight at R.T. TLC was employed to track the development of the reaction using 90% DCM and 10% CH_3OH as a mobile phase. Diethyl ether and ethanol were used to purify **4A/4B**, producing a light brownish powder for **4A** and a thick, yellowish, and oily substance for **4B**.

4A had a yield of 70% and an mp. of 119–120 °C, while **4B** had a yield of 67%. When **4A** and **4B** were investigated by ESI-MS in a positive ion approach, ions conforming to $[M + H]^+$ and $[M + Na]^+$ were detected at 319.09 m/z and 369.10 m/z, respectively. **4A** and **4B** were predicted to have molecular weights of 346 and 318 g mol^{-1}, respectively.

The infrared spectra of **4A** presented peaks at 1738 cm^{-1} (ν C=O), 725–720 cm^{-1} (ν CH_2–), 1217 cm^{-1} (ν P=O), 3100–3000 cm^{-1} (ν CH-aromatic), and 1345 cm^{-1} (C–S).

NMR: ^{1}H NMR revealed characteristic chemical shifts (d) at 3.3 (s, 3H of Ar-CH_3), d 3.4 (s, 3H of Ar-CH_3), d 2.4 (s, 3H of C]O − $\underline{CH}_3$), d 2.6 (t, 2H of $P − \underline{CH}_2$), d 2.3 (t, 2H of $P − (CH_2)_2 − \underline{CH}_2$), d 1.9 (m, 2H of P − $CH_2 − \underline{CH}_2$), 5.6 (s, 1H of solvent (CD_2CL_2)),[28] and at 7.4–7.8 (m, 8H of Ar–H) ppm. d for ^{31}P NMR (CD_2CL_2) was 32.0 ppm.

Similarly, the FTIR of **4B** displayed peaks at 1739 cm^{-1} (ν C=O), 699–710 cm^{-1} (ν CH_2), 1340 cm^{-1} (C–S–), 3100–3000 cm^{-1} (ν CH-aromatic), and 1217 cm^{-1} (ν P=O).

NMR (DMSO): ^{1}H NMR spectrum of **4B** provided chemical shifts at d 1.9 (m, 2H of P − $CH_2 − \underline{CH}_2$), 3.6 (t, 2H of $P − \underline{CH}_2$), d 3.4 (t, 2H of $\underline{CH}_2 − S − C=O$), d 2.4 (s, 3H of C]O − $\underline{CH}_3$), d 2.5 (s, 1H of solvent (DMSO)),[29] and at 7.4–7.7 ppm (m, 10H of aromatic-H).

The carbonyl group (C=O) peaks in the IR results at 1738 cm^{-1} and 1739 cm^{-1} provide evidence for the generation of compounds **4A** and **4B**, respectively. Furthermore, for **4A** and **4B**, stretching absorption was observed at 1217 cm^{-1} for P=O.[21] Furthermore, it can be seen that both **4A** and **4B** have single peaks in ^{1}H NMR at about d = 2.4 for (s, 3H of C=O − $\underline{CH}_3$), which is consistent the literature.[27,30]

The **4A** molecule was also confirmed by a strong peak at 32 ppm that was obtained from ^{31}P NMR ($CDCl_3$) analysis. Jeong *et al.* claim that oxidation and hydrogenation caused ^{31}P to shift from 24 ppm to 39 ppm, while the peak moved upfield and downfield.[31]

2.4.2 Preparation of (3-thioacetylpropyl)thiodiphenylphosphine oxide (7). Diphenylphosphinic chloride (**5**) (3.8 mmol, 0.70 ml) and 3-chloro-1-propanthiol (15 mmol, 0.33 ml) were refluxed for seven hours in DCM (6 ml). The mp. of the produced white precipitate (**6**), as indicated in Scheme 2 (Reaction 1), was 170 °C. Next, potassium thioacetate (3 mmol, 0.35 gm) and salt (**6**) (2 mmol, 0.7 gm) were combined in 11 ml of aqueous ethanol and left stirring at R.T. overnight to produce
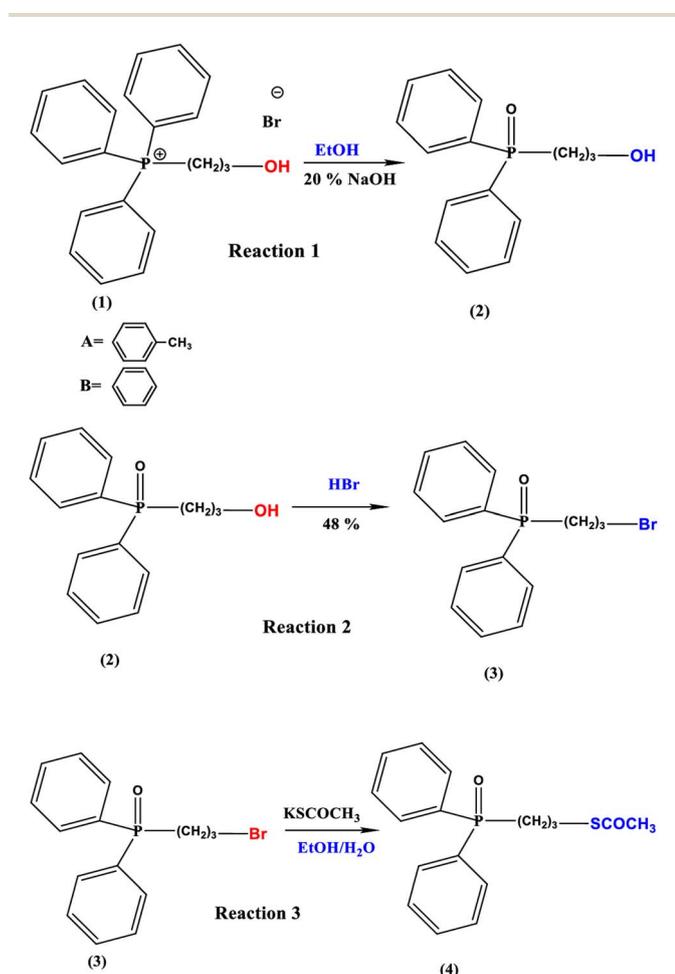
Scheme 1 Illustration of the preparation of compound **4**.
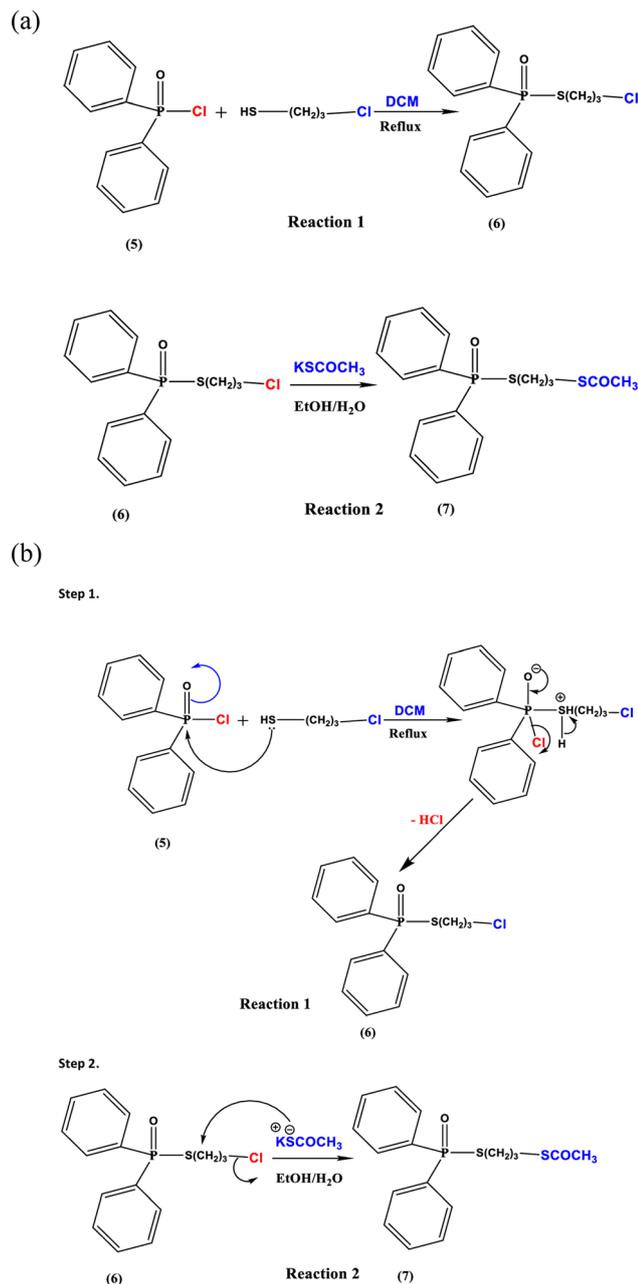
Scheme 2 (a) Illustration of the preparation of compound 7. (b) Mechanism of action.

7, as indicated in Scheme 2 (Reaction 2). Then compound 7 was purified by ether, and a beige-coloured powder was produced.

The final pure product had a mp. of 219–220 °C and was a cream-coloured powder (77% yield). The ESI-MS from a positive ion approach, with the ion conforming to $[M + H]^+$, showed a result at 351.06, and its predicted molecular weight was 350 g mol^{-1}.

The IR spectrum for 7 presented peaks at 1685 cm^{-1} (ν C=O), 3070–3000 cm^{-1} (ν CH-aromatic), 722 cm^{-1} (ν CH$_2$), 1191 cm^{-1} (ν P=O), and 1306 cm^{-1} (C–S).

NMR: ^{1}H NMR spectrum gave signals at d 5.6 (s, 1H of solvent (CD$_2$CL$_2$)) 28, d 3.4 (m, 2H of CH$_2$–), d 3.5 (t, 2H of P–S–CH$_2$–), d 3.2 (t, 2H of CH$_2$–S–C=O), d 2.4 (s, 3H of C=O–CH$_3$),

and at 7.3–7.8 ppm (m, 10H of Ar–H). These protons are influenced by strongly electron-withdrawing groups, including phosphine oxide (P=O). As expected, the shielding effect between methyl group protons in COCH$_3$ is less than that between thiol and thiol groups.[31,32]

2.4.3 Preparation of (3-thioacetylethyl-N-methylamine)-diphenylphosphine oxide (10). A yellow precipitate (9) was prepared by refluxing a combination of (2-methoxyethyl) methylamine (8) (15 mmol, 1.63 ml) and (diphenylphosphinic chloride) (5) (3.8 mmol, 0.70 ml) in 5 ml of DCM for six hours, as shown in Scheme 3 (Reaction 1). After that, potassium thioacetate (3 mmol, 0.34 gm) and salt 9 (2 mmol, 0.57 gm) were combined in 11 ml of aqueous ethanol, and the mixture was stirred overnight at R.T. under nitrogen to produce 10, as described in Scheme 3 (Reaction 2). The purification of 10 was done with EtOH to produce a yellowish powder.

A yellowish powder compound (10) was successfully prepared (85% yield), mp. 248–250 °C. The ESI-MS showed an ion conforming to $[M-(C=O)-CH_3]^+$ at 290.13 m/z, whereas its predicted molecular weight was 333 g mol^{-1}.

The IR spectra showed different peaks at 1737 cm^{-1} (ν C=O), 1375 cm^{-1} (C–S), 3100–3000 cm^{-1} (ν CH-aromatic), 1177 cm^{-1} (ν P=O), and a peak at 726–720 cm^{-1} (ν CH$_2$).

NMR: ^{1}H NMR results provided many chemical shift values at d 1.8 ppm (s, 1H, H$_2$O solvent (CDCL$_3$)), d 7.6–7.8 (m, 10H of aromatic-H), 2.4 (s, 3H of (C=O)–CH$_3$), d 3.0 (t, 2H of CH$_2$–N), 3.3 (s, 3H of N–CH$_3$), and d 3.5 (t, 2H of CH$_2$–S) ppm. d for ^{31}P NMR (CDCL$_3$) was 30.0 ppm.

4A, 4B, 7, and 10 are all well soluble in dichloromethane, chloroform, ethanol, methanol, and dimethyl sulfoxide. A single, distinct peak at 30 ppm was found by ^{31}P NMR (CDCl$_3$) analysis, indicating the formation of 10. High purity was indicated by the sharp single peaks of the compound 10.[31] The asymmetric and symmetric stretching of carbonyl (C=O) peaks appeared at 1737 cm^{-1} and 1728 cm^{-1}, respectively. The peak at 716 cm^{-1} corresponds to C=O bonding, while the peak at 1373 cm^{-1} (C–N) signifies that complete formation of ligand 10.[31] ^{1}H NMR introduced extra evidence to confirm the production of compound 10. For example, 4H at d = 3.0–3.5 ppm corresponds to (CH$_2$)$_2$ and was present in compound 10, while (CH$_2$)$_2$ was not found in the precursor material (5).

2.5 Preparation of phosphine oxide gold nanoparticle derivatives in DMSO

The technique used in this study to create biocompatible AuNPs using the current ligands in DMSO was the Turkevich method with some modifications, and they were created in a manner comparable to earlier techniques.[26] Solutions of phosphonium ligand derivatives, namely 4A, 4B, 7, and 10, (0.56 mmol, 0.4 mmol, 0.6 mmol, and 0.7 mmol, respectively), were dissolved in 20 ml of DMSO to produce AuNPs. Additionally, a solution of potassium tetrachloroaurate (KAuCl$_4$) was prepared via the addition of KAuCl$_4$ (0.8 mmol) in 9 ml of distilled H$_2$O. Then, for almost four hours at room temperature, the 4A, 4B, 7, 10, and KAuCl$_4$ solutions were combined and rapidly stirred until the colour altered from yellowish white to

(a)

Reaction 1

Reaction 2

(b)

Step 1.

Reaction 1

Step 2.
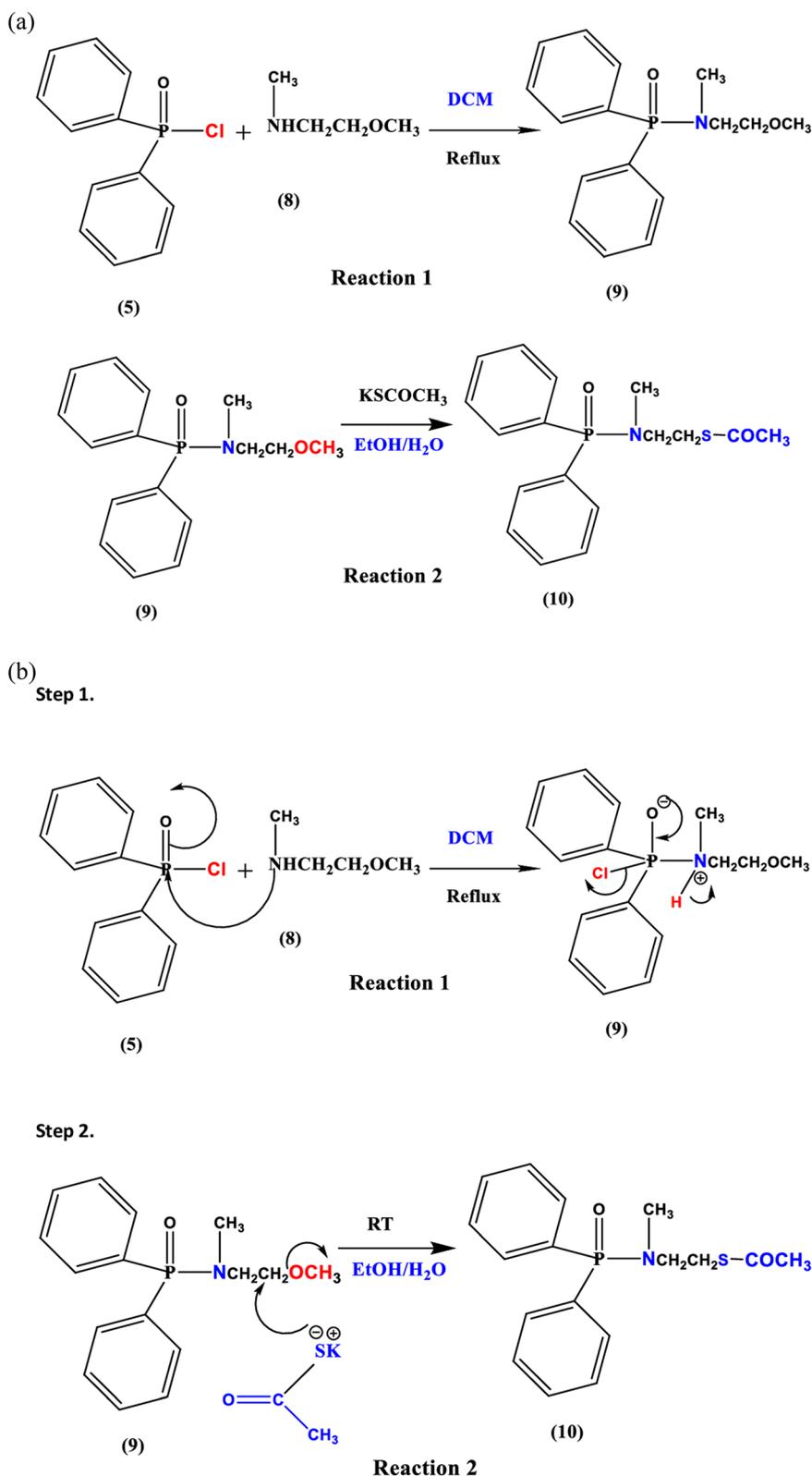
Reaction 2

Scheme 3 (a) Illustration of the preparation of compound **10**. (b) Mechanism of action.

colourless. After that, the reduction was performed by gradually adding 4 ml of NaBH$_4$ (0.4 M) to the final colourless mixture; the reaction continued under stirring for two hours, resulting in red colour, confirming the formation of AuNPs. Diethyl ether was used in liquid–liquid extractions to eliminate the extra ligands from each of the produced gold nanoparticle solutions.

Before being employed to functionalize AuNPs, all of the ligands produced in this study were characterized using ^{31}P, ^{1}H NMR, ATR-FTIR, and ESI-MS. UV-visible absorption spectroscopy, TEM, and DLS were applied to confirm the stability of **4A**-AuNPs, **4B**-AuNPs, 7-AuNPs, and **10**-AuNPs. Regular investigations of the AuNP samples were made to monitor each potential alteration, such as aggregation or agglomeration.

3.   Results and discussion

3.1   Stability of AuNPs using 4A, 4B, 7, and 10 in DMSO by using NaBH$_4$

According to Tang *et al.*, tri(*p*-tolyl)phosphine (P(*p*-tol)$_3$) AuNPs functionalized using the Brust method showed poor stability. However, replacing the ligand with 1,3 bis(diphenylphosphino) propane enhanced the stability of the AuNPs.[33] The authors confirmed that with suitable synthesis techniques, AuNPs capped with phosphine ligands can be created that are sufficiently stable for chemiresistive sensing. The significance of phosphine ligands as capping ligands toward the AuNP surface was confirmed by those results.

Notably, low NP stability results from weak interactions of phosphine ligands with metal surfaces. Because of their instability, phosphine ligands are easily exchanged with other ligands that have stronger affinity for the metal NP surface. For instance, polyphosphine ligands can be used to solve the stability problem related to phosphine ligands. Some ligands, such as di- or triphosphine, have been successfully used to stabilize palladium nanoparticles. These multiphosphine ligands coordinate strongly with palladium particles.[34]

Notably, the polarity of the P=O bond in the secondary phosphine oxide with the aryl ring is considered to be very high compared with those of aliphatic secondary phosphine oxide ligands utilized as stabilizing ligands for functionalized AuNPs.[11,29] UV-Vis spectroscopy and DLS were applied to further comprehensively characterize the synthesized AuNPs, which were mainly confirmed by a change in the colour of the dispersion solution from colourless to red.[35]

Depending on the intended application, AuNPs can be produced in a variety of sizes and surfaces. They can also be readily functionalized with biomaterials, polymers, and tiny medicinal molecules for a wide range of possible uses.[36,37] Due to their high chemical activity towards biological molecules, AuNPs can modify cellular signaling pathways and functions, based on their size effect. AuNPs were shown to be spherical by TEM imaging and can cross cell membranes because of their inherent ability to attach to sulfhydryl-bonded carbon (C–SH/R–SH) groups.[38]

Because our hydrophobic ligands are poorly soluble in water, DMSO was used to dissolve them in this investigation. Nonetheless, for over five months, these ligands showed their capacity to functionalize AuNPs in DMSO with high stability. Because of the reducing conditions, a strong covalent bond is formed on the AuNP surface that may be removing C=OCH$_3$ groups from the initial structure of the ligand to generate Ph$_2$P=O(CH$_2$)$_3$S$^-$. They can enter the lipophilic cell wall through their contact with the surface of the AuNPs.[26]

The current ligands, such as **4A** and **4B**, were chemically confirmed before being used as capping ligands. The NMR results for **4A** showed a chemical shift at d = 2.4, confirming the aliphatic methyl group (s, 3H of C=O − $\underline{CH_3}$), and at d from 1.9 to 2.6 ppm in the aliphatic zone corresponding to the chain structure of the alkyl side chain $\left(P - \underline{CH_2} - \underline{CH_2} - \underline{CH_2} \right)$. The chemical shift at about 5.6 indicates the solvent of deuterated dichloromethane (CD$_2$CL$_2$)[19] (see Fig. S1†), which confirmed the successful preparation. In the ESI-MS using the positive ion approach, ions conforming to [M + Na]$^+$ were detected at 369.10 *m/z* (Fig. S2†), where the predicted molecular weight of **4A** was 346 g mol^{-1}. In addition, the ATR-FTIR result for compound **4A** showed that the OH group in the region from 3100 to 3600 cm^{-1} was absent, while strong peaks at 1738 cm^{-1} for the carbonyl group appeared, which were not present in the starting material (see Fig. S3†).

The benzene ring in compound **4B** was used instead of the ring in toluene **4A** to compare the stability of AuNPs functionalized with these ligands. **4B** shows a single peak at chemical shift $d = 2.4$ in the ^{1}H NMR result, indicating the structure of the methyl side chain $\left(C=O - \underline{CH_3} \right)$ (see Fig. S4†), which was absent in the starting material, and the single peak of solvent DMSO occurred at d = 2.5, confirming another study.[20] The product ion spectra (Fig. S5†) of **4B** were investigated by the ESI-MS technique, where an ion conforming to [M + H]$^+$ was detected at 319.09 *m/z*, and its predicted molecular weight was 318 g mol^{-1} (Fig. S5†). The ATR-FTIR results for compound **4B** showed peaks at 1739 cm^{-1}, confirming the carbonyl grope of acetyl, which is important evidence to confirm that **4B** had been produced (Fig. S6†).

Additionally, compound 7 contains two thiol groups in its structure and exhibited the smallest size of 25 ± 6 nm among the other ligands in this study. This may be due to the presence of thiol groups, which increased its high affinity toward the surface of AuNPs. This compound was investigated by different techniques. For instance, the ^{1}H NMR spectrum gave signals at different chemical shifts that confirmed the structure of compound 7, where a new group (the methyl group of $\left(C=O - \underline{CH_3} \right)$) occurred as a single peak at d = 2.4 ppm, whereas this peak was dispersed in the starting material (Fig. S7†). ESI-MS confirmed its structure *via* the ion [M + H]$^+$ appearing at 351.06, where the predicted molecular weight of 7 was 350 g mol^{-1} (Fig. S8†). ATR-FTIR showed peaks of the carbonyl group at 1685 cm^{-1}, which were not particularly strong due to the presence of the thiol group (S), which can cause resonance with C=O, decreasing its absorption intensity (Fig. S9†).

The same procedure was undertaken for compound **10**, and the ^{1}H NMR results showed many chemical shift values. For example, new peaks appeared at d = 2.4 ppm and d = 3.5 ppm, corresponding to the methyl group $\left(C=O - \underline{CH_3} \right)$ and the methylene group that was linked to the thiol atom (t, 2H of $\underline{CH_2}$−S), respectively. In addition, a single peak of a methyl group that was linked to the nitrogen atom appeared at d = 3.3 ppm $\left(N - \underline{CH_3} \right)$ (Fig. S10†). ESI-MS showed an ion corresponding to [M-C=O–

$CH_3]^+$ at 290.13 m/z, while its expected MW was 333 g mol^{-1} (Fig. S11†). Furthermore, the IR spectra confirmed the presence of these new functional groups at different peaks of 1737 cm^{-1} (ν C=O) and 1375 cm^{-1} (C–S) (Fig. S12†). These findings indicate the successful synthesis of the current compounds. Due to their high purity, the gold nanoparticles coated with these compounds were homogeneous with good stability.

Despite modifying the synthesis conditions, such as varying the concentrations of ligand and gold salt, multiple attempts failed to synthesize phosphonium AuNPs employing the present capping ligands using the two-phase H$_2$O/DCM approach.[26]

Conversely, as soon as NaBH$_4$ was incorporated into the combined solutions, aggregation and coagulation of the bulk gold took place. The reason for this aggregation may have resulted from the low affinity of gold nanoparticles for two phases solvent (H$_2$O/ DCM). The characteristics of the ligands not only made the AuNPs stable but also increased their solubility in non-polar and polar solvents.[39]

After preparing homogeneous AuNPs in DMSO, Au^{+3} (III) was reduced to Au^0 with NaBH$_4$ in the presence of **4A/4B**, **7**, or **10**. This reduction technique produced red-coloured dispersed AuNPs functionalized with all the mentioned ligands that remained stable for almost five months without showing any obvious signs of aggregation.

3.2 UV-visible results

The occurrence of a sharp peak at about 520 nm in the UV-visible spectrum for the fresh and aged solutions provided proof of the production of AuNPs. This result indicates that the particle size ranged from 5 nm to 10 nm, based on the results for comparable thiolate ligand-capped AuNPs documented in a previous study.[40] Additionally, AuNPs were identified through a peak in the UV-Vis spectra at 520–535 nm, which is a sign of evenly distributed spherical nanoparticles between 1 and 20 nm.[41] Fig. 1–4 display the stability of the AuNPs over five months. UV-visible spectroscopy provided evidence that AuNPs

were formed in DMSO using the reduction procedure. The UV-Vis spectra at the initial time (time) revealed bands at 547 nm, 530 nm, 527 nm, and 529 nm for AuNPs stabilized by **4A**, **4B**, **7**, and **10**, respectively, as shown in Fig. 1–4.

In this study, slight differences in the surface plasmon resonance (547 nm, 530 nm, 527 nm, 529 nm) of **4A**-AuNPs, **4B**-AuNPs, **7**-AuNPs, and **10**-AuNPs were observed, as shown in Fig. 1–4, respectively. In terms of stability, **10**-AuNP and **4A**-AuNP remained stable for only 3 months, while **4B**-AuNPs and **7**-AuNPs were stable for 5 months. For **10**-AuNPs, tertiary amines are no longer in a proton state and aggregate more quickly than thiol-capping ligands. This could be the reason for the faster growth in the size of the AuNPs and lower stability; such behaviour was noticed in earlier studies.[42] The presence of a tolyl group in **4A** is no more beneficial for the stability of the AuNPs than other compounds that contain benzene groups. This is evidenced by
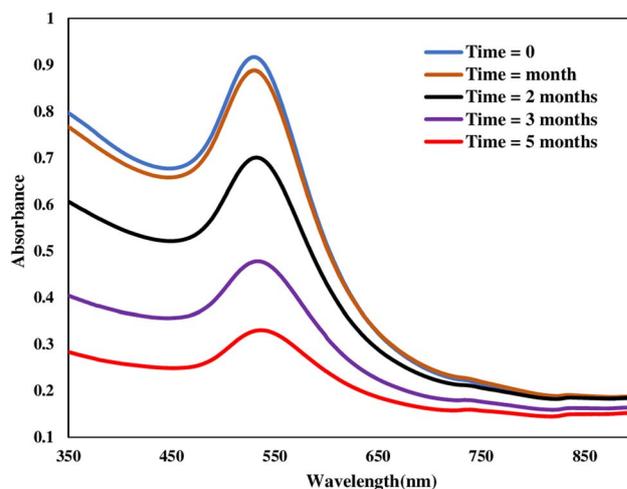

Fig. 2 UV-Vis absorption spectra of AuNPs capped by **4B** as a protecting ligand in DMSO. The different UV-Vis spectra signify these AuNPs at different times.
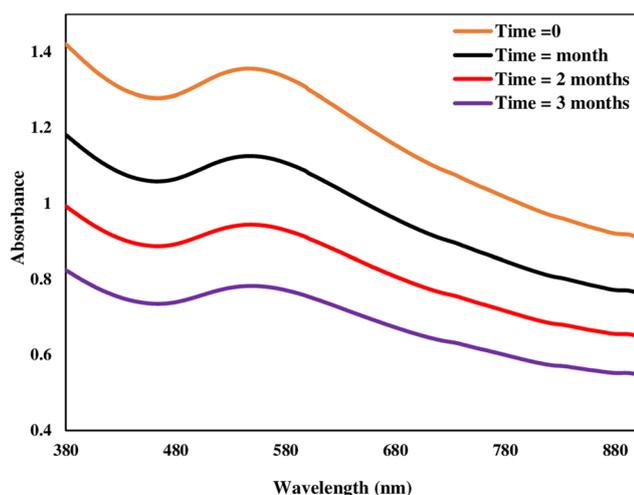

Fig. 1 UV-Vis absorption spectra of homogenous AuNPs capped by **4A** acting as a protective ligand. These AuNPs were distributed in DMSO at a variety of times (from 0 to 3 months).
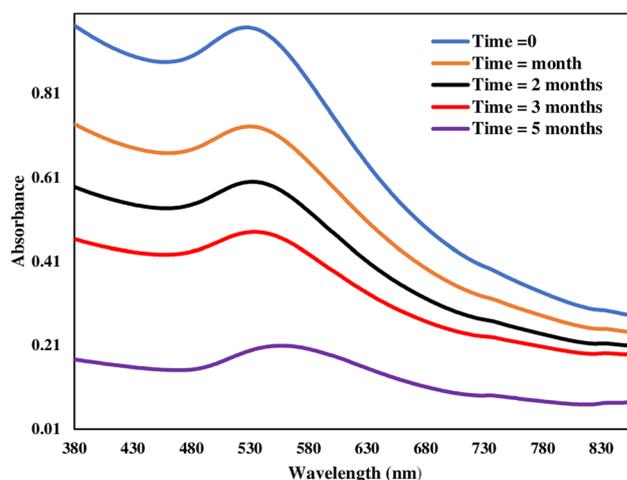

Fig. 3 UV-Vis absorption spectra of dispersed AuNPs functionalized by ligand **7**. The various UV-Vis spectra were measured at various times.
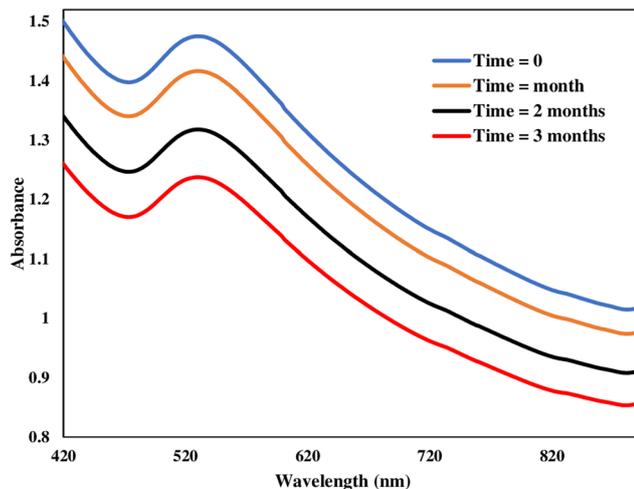
Fig. 4 UV-Vis absorption spectra of AuNPs functionalized by **10**. The various UV-Vis spectra were measured at various times.

the wider gold size distributions in **4A**-AuNPs, which is explained by TEM in the next section. The changes in surface plasmon resonance (SPR) and the absorbance of all types of produced AuNPs over time are shown in Table 1 and Scheme 4, respectively. From Table 1, we can see that the absorbance shifted towards longer wavelength, representing a redshift over time. In Scheme 4, we can see that the absorbance of **10**-AuNPs and **4A**-AuNPs decreased linearly, suggesting lower stability of the initial size. This is evidenced by the DLS measurement in the next section, where minimum changes (increments) in the sizes of the AuNPs take place in the case of **7**-AuNPs, followed by **4B**-AuNPs, **10**-AuNPs, and **4A**-AuNPs after 3 months. The absorbance of **4B**-AuNPs and **7**-AuNPs decreased cubically, suggesting lower and slower changes (increments) in the size of the AuNPs. Similar alterations were observed in the case of silver nanoparticles in an earlier investigation.[43]

3.3 Dynamic light scattering results

Dynamic light scattering (DLS) also examined the homogenous AuNPs capped with **4A**, **4B**, **7**, and **10** ligands. All four samples of AuNPs displayed spherical-shaped particles. The lowest size of AuNPs capped by ligand **7**, which contains two thiol groups, and their great stability for five months demonstrates the importance of the dithiol group in enhancing the stability of AuNPs, as established by previous research.[40,44]

According to Fig. 5A, B and 6C and D, the mean diameters of the **4A**-AuNPs, **4B**-AuNPs, **7**-AuNPs, and **10**-AuNPs samples were

78 ± 11 nm, 59 ± 9 nm, 37 ± 8 nm, and 68 ± 9 nm, respectively. The DLS results for the AuNPs were consistent with the UV-Vis results, confirming each other.

The UV-Vis spectra revealed that the AuNPs functionalized by **4A** had slightly larger surface plasmon resonance (SPR) at 547 nm among those functionalized by other ligands in this study. This suggests that they would lose their colloidal stability and aggregate after approximately three months, whereas **4B**-AuNPs remained stable for more than five months with no apparent aggregation, as evidenced by DLS and UV-Vis results. The size of **4A**-AuNPs was 78 ± 9 nm, which changed to 255 ± 12 nm based on the DLS results, demonstrating that the large size formed approximately after 3 months. This larger size suggests the presence of agglomeration (where the nanoparticles are loosely bonded). However, there was no indication of any aggregation (nanoparticles have a strong bond between them). Similarly, the size of **4B**-AuNPs gradually changed from 59 ± 9 nm at the initial time to 106 ± 15 nm after 3 months and to 164 ± 11 nm approximately after 5 months, indicating an increase in size and size distribution (Fig. 5B).

In addition, the size of **7**-AuNPs was the smallest (37 ± 8 nm) at the initial time, and it remained stable for more than 5 months; it gradually increased to 58.8 ± 8 nm after 3 months and to 65 ± 12 nm after 5 months. These findings confirm that (3-thioacetylpropyl)thiodiphenylphosphine oxide (**7**) has high affinity toward the surface of gold nanoparticles (see Fig. 6C).

Gold nanoparticles functionalized by ligand **10** also showed a narrow peak with quite good stability and nanoscale size range. The size of **10**-AuNPs was 68 ± 9 nm initially, which increased to 122 ± 11 nm after 3 months. Thus, all the DLS results confirm the successful preparation of AuNPs in our study.

3.4 Transmission electron microscopy results

The samples of **4A**-AuNPs, **4B**-AuNPs, **7**-AuNPs, and **10**-AuNPs were also analyzed by Transmission electron microscopy (TEM). Fig. 7 exhibits the good monodispersed and spherical shape distribution of the AuNPs. Well-defined shape and narrow size are observed in the case of **4B**-AuNPs, **7**-AuNPs, and **10**-AuNPs with diameters of 40 ± 8 nm, 25 ± 6 nm, and 43 ± 7 nm, respectively. However, a big size with quite a wide distribution (55 ± 13.6 nm, Fig. 7A) is observed in the case of **4A**-AuNPs, ensuring polydispersity. Ligand **4A**, which contains tolyl groups instead of benzene, may have low affinity towards the surface of AuNPs in comparison to ligand **4B**. These findings confirm that the type of ligand attached to the nanoparticle surface plays a vital role in changing the properties of the nanoparticles, in agreement with previous studies.[34,45]

Table 1 Comparison of the SPR of **4A**-AuNPs, **4B**-AuNPs, **7**-AuNPs, and **10**-AuNPs at the initial time and after several months

Name of AuNPs	SPR (nm) at an initial time	In the first month	In the second month	In the third month	In the fifth month
4A-AuNP	547 nm	552 nm	555 nm	566 nm	—
4B-AuNP	530 nm	535 nm	537 nm	541 nm	544 nm
7-AuNP	527 nm	533 nm	538 nm	542 nm	560 nm
10-AuNP	529 nm	531 nm	536 nm	540 nm	—
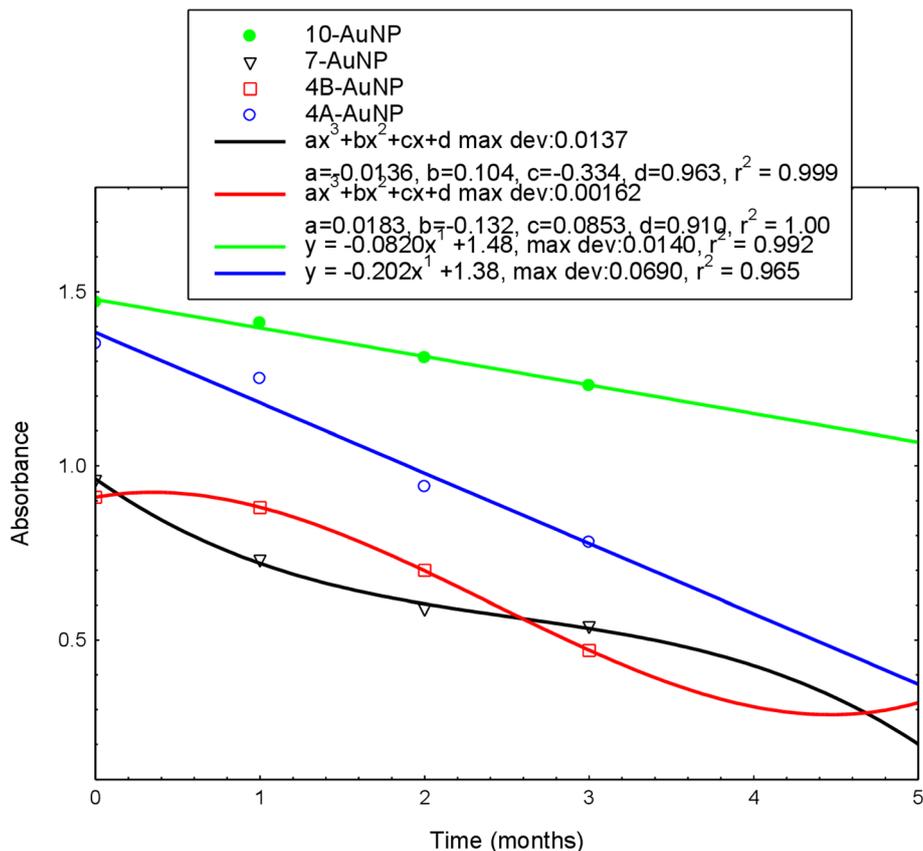
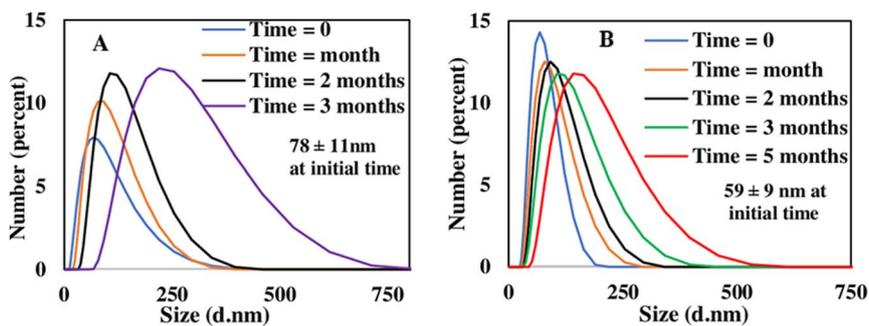**Scheme 4** Variation in peak absorbance with time.

Fig. 5 The size of **4A**-AuNPs (A) and **4B**-AuNPs (B) and their standard deviation using DLS measurements performed at 3 and 5 months, respectively.
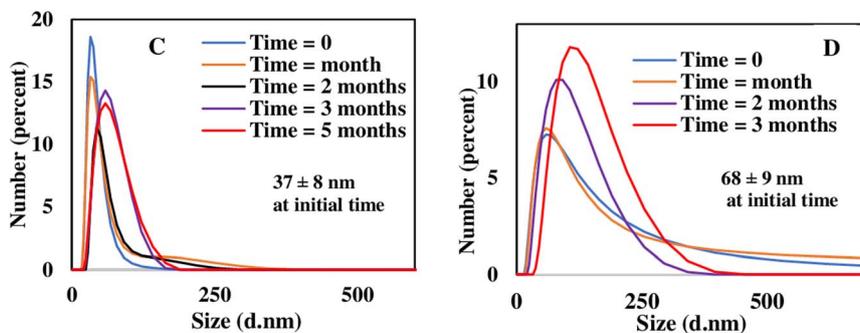

Fig. 6 The size of **7**-AuNPs (C) and **10**-AuNPs (D) and their standard deviation. DLS measurements were conducted at various times.
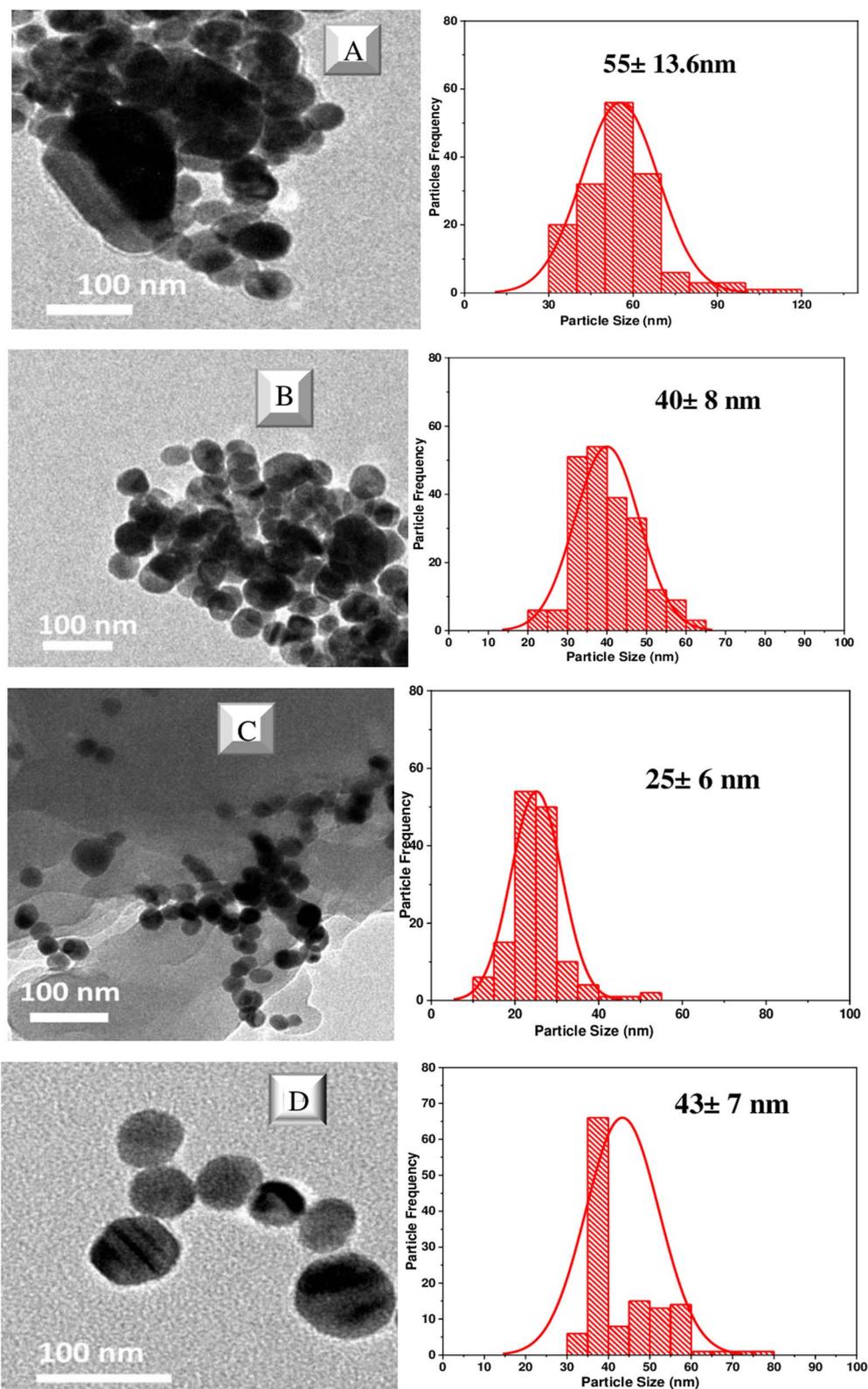
Fig. 7 Representative TEM micrographs of cationic phosphonium **4A**-AuNPs (A), **4B**-AuNPs (B), **7**-AuNPs (C), **10**-AuNPs (D) at the initial time (freshly prepared), and corresponding particle size histograms, where ligand **4A**, **4B**, **7**, and **10** compounds are used as protecting ligands in DMSO.

According to the literature, the lower stability of the nanoparticles results from the poor interactions of phosphine ligands with the metal surfaces. Due to their instability, phosphine ligands are easily swapped out for ligands that have stronger affinity for the metal. Phosphine ligands are completely replaced with other types of ligands through straightforward processes, in contrast to the ligand exchange of thiol-passivated gold nanoparticles. Ligands containing phosphines with thiols greatly enhance the stability of the AuNPs. In contrast, other ligands that contain phosphines with amines produce less stable AuNPs.[34] Here, the TEM results revealed that ligands containing thiol and phosphine groups were effective in preventing agglomeration/aggregation and achieving diffusion-controlled growth mechanisms of gold nanoparticles.

4. Conclusions

Gold nanoparticles (AuNPs) were successfully stabilized using phenylphosphine derivatives, providing excellent control over their stability and size. To the best of our knowledge, this research represents the first synthesis of AuNPs employing the newly introduced protective ligands **4A**, **4B**, **7**, and **10** with a reduction process in dimethyl sulfoxide (DMSO). The ligands were found to strongly bind with the AuNP surface, exhibiting air stability, which can be attributed to their high solubility in DMSO. The characteristics of this approach include the ability to control nanoparticle size through modification of ligand composition. For example, varying the phenyl ring in **4B** with a tolyl ring in **4A** resulted in distinct AuNP sizes and stability profiles, demonstrated by different UV-Vis absorbance peaks at 547, 530, 527, and 529 nm.

Stability over time was also evident, with **7**-AuNPs and **4B**-AuNPs remaining highly stable for up to five months, whereas **4A**-AuNPs and **10**-AuNPs remained stable for three months. This stability, observed through UV-Vis, DLS, and TEM analyses, indicates that the synthesis method yields robust and consistent AuNPs with well-defined sizes and minimal agglomeration. The TEM results are consistent with the DLS and UV results. For instance, **4A**-AuNPs, **4B**-AuNPs, **7**-AuNPs, and **10**-AuNPs are produced with diameters of 55 ± 13.6 nm, 40 ± 8 nm, 25 ± 6 nm, and 43 ± 7 nm, respectively.

However, there are certain limitations. While the ligands demonstrate stability, the variation in stability across different AuNPs, especially with **4A**-AuNPs and **10**-AuNPs, highlights the need for further optimization of ligand structures to achieve uniform long-term stability. Additionally, the reliance on DMSO in the process limits its scalability due to concerns about the solvent's environmental effects and toxicity. The nanoparticle sizes also vary, which could be a limitation for certain applications that require uniformity.

Future directions in this field include exploring alternative and more environmentally friendly solvents for synthesizing AuNPs. Further studies could focus on precise control over nanoparticle size and stability by tuning the ligands or using a combination of protective agents. Additionally, the application of these stabilized AuNPs in biomedicine, particularly in photothermal therapy for cancer treatment, warrants further investigation, including *in vivo* studies to assess their therapeutic efficacy and safety.

In conclusion, the combination of phenylphosphine derivatives and DMSO in the synthesis of AuNPs offers promising advances in nanoparticle stability and size control. This work paves the way for future developments in the use of gold nanoparticles for medical applications, with the potential to enhance therapeutic strategies in cancer treatment.

Data availability

The data can be made available at the request of the authors.

Author contributions

W. A. M.: supervision, conceptualization, methodology, writing– original draft, data curation, formal analysis, writing–review & editing., M. M. A.: resources, investigation. P. S.: resources, software, formal analysis. A. B.: funding acquisition, visualization, writing–review & editing.

Conflicts of interest

The authors declare that they have no conflicts of interest, financial or otherwise, that could have influenced the research presented in this paper.

Acknowledgements

References

1 J. Zhao, S. C. Nguyen, R. Ye, B. Ye, H. Weller, G. A. Somorjai, A. P. Alivisatos and F. D. Toste, *ACS Cent. Sci.*, 2017, **3**, 482–488.

2 M. Choudhary, S. Siwal, D. Nandi and K. Mallick, *Appl. Surf. Sci.*, 2017, **424**, 151–156.

3 N. Bloise, A. Massironi, C. Della Pina, J. Alongi, S. Siciliani, A. Manfredi, M. Biggiogera, M. Rossi, P. Ferruti, E. Ranucci and L. Visai, *Front. Bioeng. Biotechnol.*, 2020, **8**, DOI: **10.3389/fbioe.2020.00132**.

4 J. Georgeous, N. AlSawaftah, W. H. Abuwatfa and G. A. Husseini, *Pharmaceutics*, 2024, **16**, 1332.

5 J. Ping, D. Zhao and C. Tianrui, *Advances in Engineering Research*, Atlantis Press, 2015, pp. 44–46.

6 S. Sortino, *J. Mater. Chem.*, 2011, **22**, 301–318.

7 N. Lalwani, Y.-S. Chen, G. Brooke, N. A. Cross, D. W. Allen, A. Reynolds, J. Ojeda, G. J. Tizzard, S. J. Coles and N. Bricklebank, *Chem. Commun.*, 2015, **51**, 4109–4111.

8 L. Gentile, H. Mateos, A. Mallardi, M. Dell'Aglio, A. De Giacomo, N. Cioffi and G. Palazzo, *J. Nanopart. Res.*, 2021, **23**, 35.

9 S. J. Amina and B. Guo, *IJN*, 2020, **15**, 9823–9857.

10 R. H. Adnan, J. M. L. Madridejos, A. S. Alotabi, G. F. Metha and G. G. Andersson, *Advanced Science*, 2022, **9**, 2105692.

11 S. Jin, W. Du, S. Wang, X. Kang, M. Chen, D. Hu, S. Chen, X. Zou, G. Sun and M. Zhu, *Inorg. Chem.*, 2017, **56**, 11151–11159.

12 B. K. Malviya, V. P. Verma and S. Sharma, *Org. Biomol. Chem.*, 2021, **19**, 9491–9500.

13 N. T. K. Thanh and L. A. W. Green, *Nano Today*, 2010, **5**, 213–230.

14 M.-A. Neouze and U. Schubert, *Monatsh. Chem.*, 2008, **139**, 183–195.

15 C. Thambiliyagodage, *Curr. Res. Green Sustainable Chem.*, 2022, **5**, 100245.

16 S. R. Samanta, R. Kulasekharan, R. Choudhury, P. Jagadesan, N. Jayaraj and V. Ramamurthy, *Langmuir*, 2012, **28**, 11920–11928.

17 I. Cano, M. A. Huertos, A. M. Chapman, G. Buntkowsky, T. Gutmann, P. B. Groszewicz and P. W. N. M. van Leeuwen, *J. Am. Chem. Soc.*, 2015, **137**, 7718–7727.

18 I. Cano, L. M. Martínez-Prieto, P. F. Fazzini, Y. Coppel, B. Chaudret and P. W. N. M. van Leeuwen, *Phys. Chem. Chem. Phys.*, 2017, **19**, 21655–21662.

19 P. Fiurasek and L. Reven, *Langmuir*, 2007, **23**, 2857–2866.

20 I. Cano, A. M. Chapman, A. Urakawa and P. W. N. M. van Leeuwen, *J. Am. Chem. Soc.*, 2014, **136**, 2520–2528.

21 B. J. Borah, A. Yadav and D. K. Dutta, *J. Biomed. Nanotechnol.*, 2011, **7**, 152–153.

22 J. R. Dilworth and N. Wheatley, *Coord. Chem. Rev.*, 2000, **199**, 89–158.

23 J. Zhou, J. Ralston, R. Sedev and D. A. Beattie, *J. Colloid Interface Sci.*, 2009, **331**, 251–262.

24 M. J. MacLeod, A. J. Goodman, H.-Z. Ye, H. V.-T. Nguyen, T. Van Voorhis and J. A. Johnson, *Nat. Chem.*, 2019, **11**, 57–63.

25 P. Wand, J. D. Bartl, U. Heiz, M. Tschurl and M. Cokoja, *J. Colloid Interface Sci.*, 2016, **478**, 72–80.

26 Y. Ju-Nam, N. Bricklebank, D. W. Allen, P. H. E. Gardiner, M. E. Light and M. B. Hursthouse, *Org. Biomol. Chem.*, 2006, **4**, 4345–4351.

27 Y. Ju-Nam, D. W. Allen, P. H. E. Gardiner and N. Bricklebank, *J. Organomet. Chem.*, 2008, **693**, 3504–3508.

28 G. R. Fulmer, A. J. M. Miller, N. H. Sherden, H. E. Gottlieb, A. Nudelman, B. M. Stoltz, J. E. Bercaw and K. I. Goldberg, *Organometallics*, 2010, **29**, 2176–2179.

29 H. E. Gottlieb, V. Kotlyar and A. Nudelman, *J. Org. Chem.*, 1997, **62**, 7512–7515.

30 O. N. Kononova, K. A. Shatnykh, K. V. Prikhod'ko and D. M. Kashirin, *Russ. J. Phys. Chem.*, 2009, **83**, 2340–2345.

31 K. U. Jeong, J.-J. Kim and T.-H. Yoon, *Polymer*, 2001, **42**, 6019–6030.

32 D. Kim, S. Salman, V. Coropceanu, E. Salomon, A. B. Padmaperuma, L. S. Sapochak, A. Kahn and J.-L. Brédas, *Chem. Mater.*, 2010, **22**, 247–254.

33 C. Tang, K. H. Ku, S.-X. Lennon Luo, A. Concellón, Y.-C. M. Wu, R.-Q. Lu and T. M. Swager, *ACS Nano*, 2020, **14**, 11605–11612.

34 J. Choi and B. H. Kim, *Nanomaterials*, 2024, **14**, 1685.

35 Y. Wang, X.-H. Liu, R. Wang, B. Cula, Z.-N. Chen, Q. Chen, N. Koch and N. Pinna, *J. Am. Chem. Soc.*, 2021, **143**, 9595–9600.

36 I. Ielo, G. Rando, F. Giacobello, S. Sfameni, A. Castellano, M. Galletta, D. Drommi, G. Rosace and M. R. Plutino, *Molecules*, 2021, **26**, 5823.

37 N. Valatabar, F. Oroojalian, M. Kazemzadeh, A. A. Mokhtarzadeh, R. Safaralizadeh and A. Sahebkar, *J. Nanobiotechnol.*, 2024, **22**, 386.

38 M. Singh, N. Chandrasekaran, A. Mukherjee, M. Kumar and A. K. Kumaraguru, *Bioprocess Biosyst. Eng.*, 2014, **37**, 1859–1869.

39 R. A. Sperling and W. J. Parak, *Philos. Trans. R. Soc., A*, 2010, **368**, 1333–1383.

40 S. Khodami, M. Gharakhloo, S. Dagdelen, P. Fita, J. Romanski, M. Karbarz, Z. Stojek and M. Mackiewicz, *ACS Appl. Mater. Interfaces*, 2024, **16**, 57659–57671.

41 J. Santhoshkumar, S. Rajeshkumar and S. Venkat Kumar, *Biochem. Biophys. Rep.*, 2017, **11**, 46–57.

42 A. Heuer-Jungemann, N. Feliu, I. Bakaimi, M. Hamaly, A. Alkilany, I. Chakraborty, A. Masood, M. F. Casula, A. Kostopoulou, E. Oh, K. Susumu, M. H. Stewart, I. L. Medintz, E. Stratakis, W. J. Parak and A. G. Kanaras, *Chem. Rev.*, 2019, **119**, 4819–4880.

43 W. Abdussalam-Mohammed, K. Edbey, H. E. Farhat, P. Shah, S. S. Shamsi and A. Bhattarai, *Inorg. Chem. Commun.*, 2025, **173**, 113893.

44 R. Tang, R. A. Hughes, W. J. Tuff, A. Corcoran and S. Neretina, *Nanoscale Adv.*, 2024, **6**, 3632–3643.

45 J. C. Burgos, S. M. Mejía and G. F. Metha, *ACS Omega*, 2019, **4**, 9169–9180.